Evaluation of side spillage for a hypersonic air intake using computational fluid dynamic techniques

Afroz Javed and Debasis Chakraborty

Abstract

Mass capture ratio of a hypersonic air intake is one of the most important performance parameters. However, no a priori estimate of its value exists for use in initial design exercise of a hypersonic vehicle. In the present work, an air intake of a non-axisymmetric scramjet engine, designed using stream thrust methodology, is studied using computational fluid dynamic techniques. A large amount of air mass flow rate is observed to spill from the sides, which is not accounted for in the initial design phase. In absence of even an approximate estimate of this spillage, computational fluid dynamic studies become the only available tool to evaluate the mass capture ratio. Simulations are also carried out with a side wall at the intake to stop spillage. Although mass capture ratio and static pressure at combustor entry improve, deterioration in other flow parameters such as static temperature, Mach number and total pressure is observed.

Introduction

For hypersonic air breathing vehicles, the mass capture ratio is an important parameter as the amount of air that flows through the projected frontal area without entering the engine(s) does not do any work and incurs a drag penalty that must be overcome by the propulsion system. The difference between the free stream air mass flow that could pass through the projected area and the flow area of the free stream that actually enters the physical opening is called spillage. The intakes are designed in such a way that the first oblique shock impinges on the lip of the physical entrance of the vehicle internal flow path. At Mach numbers below the design Mach number, the shock on lip condition is not met and there is occurrence of spillage depending on the difference between flight and design Mach numbers. For axisymmetric intakes, it is possible to have a design Mach number with zero spillage.

One of the most widely used methodology for the design and initial performance estimation of scramjet engines is stream thrust analysis, reported by Curran and Craig.[1] The method is further explained in detail by Heiser and Pratt.[2] Several authors[3–5] have used this methodology for the preliminary design and performance analysis of hypersonic airbreathing engines. However, stream thrust methodology being one dimensional (1D) in nature does not address the issue of the side spillage of the air mass flow. Initial design calculations using stream thrust analysis for a non-axisymmetric scramjet vehicle does not give reliable estimates. This unreliability in the estimates of side spillage necessitates use of Computational Fluid Dynamics (CFD) at an early design stage itself.

Non-axisymmetric intakes are analysed using CFD by many researchers[6–12] for their performance in terms of pressure drops and mass flow ratios. However, these studies are carried out by considering two-dimensional (2D) domains without addressing the issue of side spillage. Only a few studies[13–16] are carried out to analyse the phenomenon of side spillage. A combined experimental and CFD study carried out by Nguyen et al.[13] has shown a less than 4% difference for mass capture ratios predicted by CFD and those obtained experimentally. Nair et al.[14] have carried out Reynold's Averaged Navier Stokes (RANS) simulations for a 2D intake without side walls and reported a spillage of nearly 27% of air mass flow from the sides at design Mach number. Various

Directorate of Computational Dynamics Defence Research and Development Laboratory, Hyderabad, India

Corresponding author:
Afroz Javed, Directorate of Computational Dynamics, Defence Research and Development Laboratory, APJ Abdul Kalam Missile Complex, Kanchanbagh, Hyderabad, Telangana 500058, India.
Email: afrozjaved@gmail.com

intake geometries with and without side walls have been studied numerically through RANS simulations by Krause and Ballmann.[15] It is shown that the mass spillage for the intake with side walls is around 21% while that for without side wall is 44%. Tani et al.[16] have carried out experimental and numerical studies for the effect of side spillage on the performance of a scramjet powered vehicle which shows a 15% reduction of thrust occurs with side spillage as compared with a model having side walls. For the mission considered in these studies, there is a 60% reduction in the payload value due to thrust reduction caused by side spillage.

It can be observed that the side spillage for non-axisymmetric intakes is significant. The introduction of side walls does reduce side spillage but it still remains considerable. Side spillage is not at all accounted for in the stream thrust analysis method. Hence, it becomes erroneous to use the stream thrust analysis method for initial design process of a scramjet engine with non-axisymmetric intake.

In the present study, an attempt is made to study the difference in mass capture ratios calculated by using the stream thrust methodology and that computed using three-dimensional (3D) CFD analysis. The results are analysed to bring out the deficiencies in the stream thrust analysis method used by many researchers[3–5] for initial design analysis of non-axisymmetric intakes for scramjet engines. The effect of presence of intake side walls on the mass capture ratio is also investigated computationally. To carry out this study, non-reacting CFD simulations are performed for a scramjet engine intake, which is designed using stream thrust methodology.

Flight conditions and the geometry

The scramjet engine under consideration is designed to fly at an altitude of 30 km with a flight Mach number of 6.5. These design conditions are summarised in Table 1. The scramjet engine has a mixed compression (external internal) intake with a span of 380 mm. The intake has two ramps which give rise to the formation of two external oblique shocks converging at the cowl lip (lower portion of the physical entrance). The third oblique shock occurs from the lip and impinges at the end of the second ramp making the flow parallel to the engine flow path. The flow is further compressed internally by a converging section which is followed by a constant area isolator. A schematic drawing of the scramjet engine is shown in Figure 1. For the 3° angle of attack, ideal intake mass flow rate at design conditions comes out to be 9.15 kg/s.

Computational domain and grids

Half of the geometry is modelled due to symmetry in the pitch plane passing through the middle of the scramjet engine span. The computational domain is shown in Figure 2 with different boundary locations. Sufficient space is given around the intake to contain shocks emanating from the leading edge and flow due to side spillage. ICEM CFD[17] software is used for making hexahedral grids with boundary layers near the walls and clustering near shock locations. Three different grid sizes of 5.0, 9.0 and 14.0 million were

Table 1. Design flight conditions.

Parameter	Value
Flight Mach number	6.5
Flight altitude	30 km
Atmospheric temperature	226.6 K
Atmospheric pressure	1196 Pa
Angle of attack	3°
Flight speed	1961 m/s
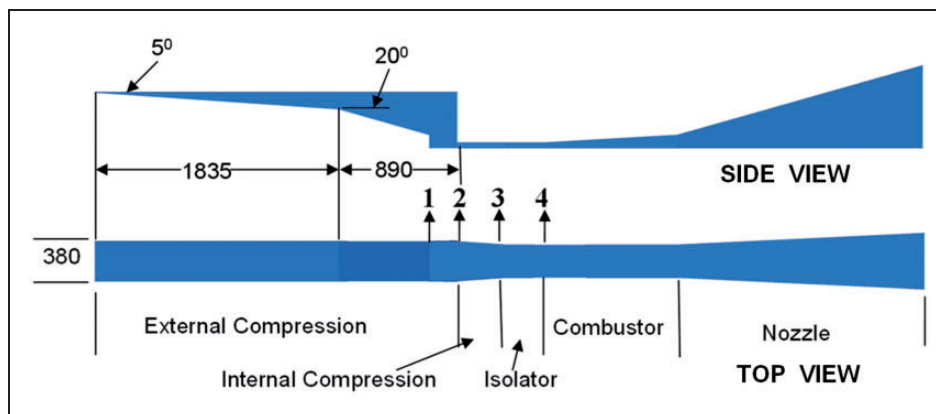
Figure 1. Schematic of the scramjet vehicle showing details of the intake portion. Station No. 1: Start of Cowl; Station No. 2: End of 20° Ramp; Station No. 3: End of Internal Compression and Station No. 4: End of Isolator.

considered; the average static pressure values at plane 4 (after isolator) are evaluated to be 91,170, 97,240 and 97,560 Pa, respectively. With these average static pressure variations, 9.0 million grid is considered to have sufficient resolution and used for further analysis. The maximum y^+ in the boundary layer region is around 4.0 for this grid size. A view of the grid in symmetry plane is shown in Figure 3.

Computational details

A commercial software ANSYS CFX 11[18] is used to solve 3D RANS equations along with $k–\varepsilon$ turbulence model[19] with a second-order spatially accurate scheme. To find out the accuracy and the range of applications, the software was extensively validated for various flow fields including flow in the rectangular duct behind backward facing step,[20,21] base flow,[22] free jets,[23] free stream and jet interaction,[24,25] dual pulse rocket motor,[26] air intakes,[27] scramjet engines,[28,29] etc. and very good quantitative agreement between experimental and computational results was obtained.

Boundary conditions

The flow conditions at different boundary locations are given as follows. Supersonic velocity, static pressure and static temperature are applied at inlet. Static pressure boundary condition is applied at the outlet. The walls are adiabatic with no slip velocity boundary conditions. Table 2 shows all the parameters applied at the boundaries. Atmospheric air is assumed to be a mixture of 77% Nitrogen and 23% Oxygen (by mass) with thermal and transport properties varying with local temperature.

Numerical simulations

A second-order spatially accurate scheme[18] is used to carry out steady state simulations. A physical time step of 1×10^{-6} s is used. Log normalised residue of 10^{-4} with global imbalances in mass, momentum and energy lower than 0.5% is considered as convergence criteria.

Results and discussion

The distribution of Mach number in the symmetry plane of intake region is shown in Figure 4. The oblique shocks from the nose of intake and second ramp can be clearly seen in the figure. These oblique shocks do not intersect exactly at cowl lip due to presence of boundary layer. This effect of boundary layer can be seen in the start of second oblique shock also which does not start exactly at the turning point between first and second ramps. The third oblique shock starts from the cowl lip and reaches the end of second ramp. The positions of the shocks can be
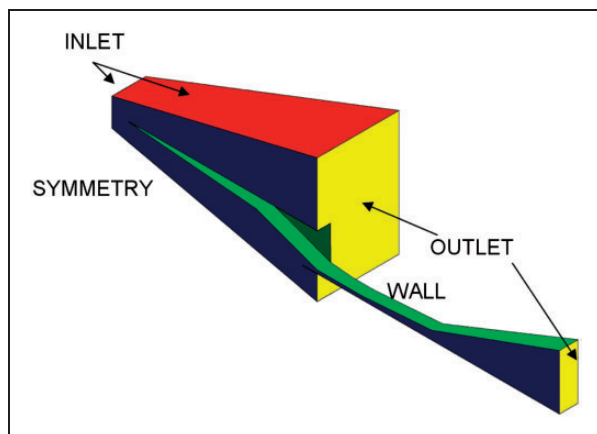
Figure 2. Computational domain and boundary locations.

Table 2. Boundary values for the simulation.

Boundary	Parameters
Inlet	Supersonic velocity
	Axial component = 1961 cos 3° m/s
	Vertical component = 1961 sin 3° m/s
	Spanwise component = 0 m/s
	Static pressure = 1196 Pa
	Static temperature = 226.6 K
Outlet	Static pressure = 1196 Pa
Walls	Heat transfer = 0
	Velocity = 0
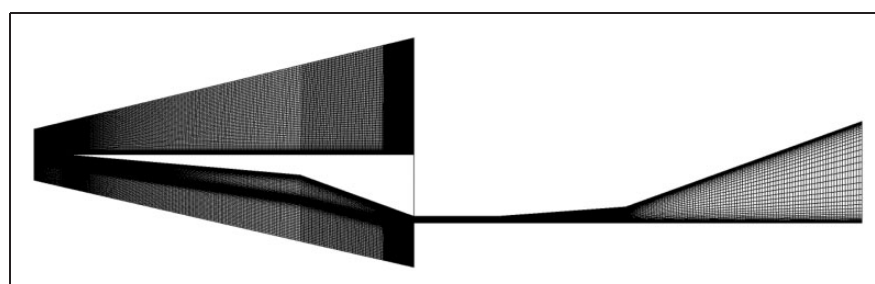
Figure 3. View of grids in symmetric plane.
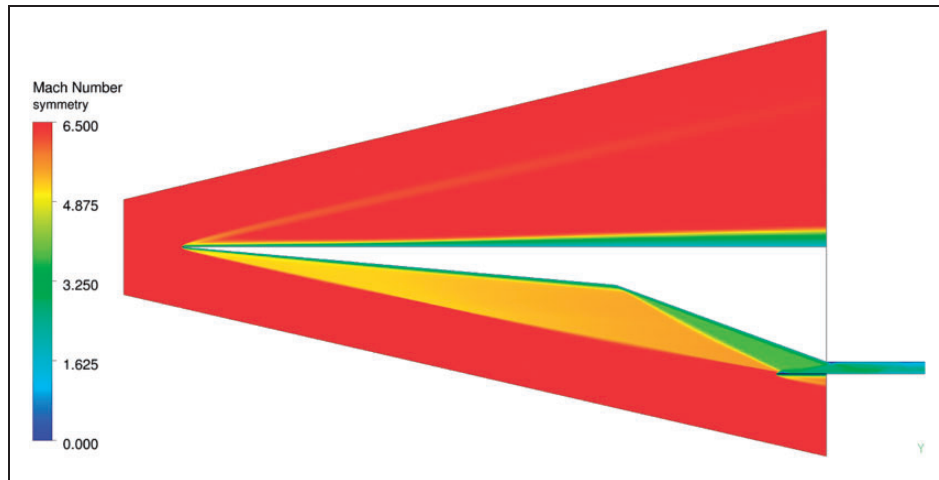
Figure 4. Mach number distribution in symmetry plane.
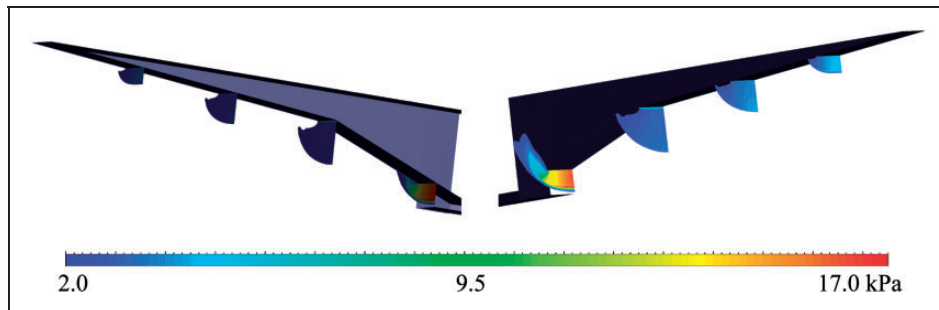
Figure 5. Static pressure distribution in span wise planes.
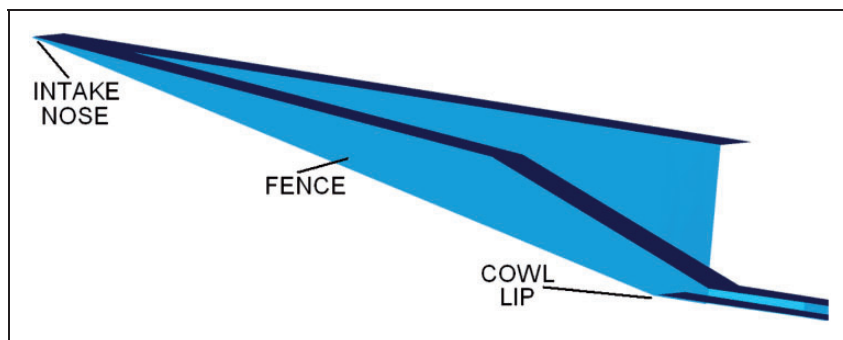
Figure 6. Schematic geometry of the intake with side fence.

clearly observed to be away from the geometric turn-ings due to viscous effects.

Another view of the flow field in terms of static pressure distribution in span wise planes is shown in Figure 5. An examination of Figure 5 indicates that the static pressure rise 'spills' beyond the span bound-ary of the air intake, being a cause for the physical spillage of the flow. The mass flow rate of the air at the engine physical entrance is found to be 6.238 kg/s, as against 9.15 kg/s by 1D calculation. The intake cap-ture ratio at the design point is 68.17%. Earlier simu-lations carried out for a hypersonic intake by Nair et al.[14] indicate that the difference between the mass flow rates evaluated through solving Euler equations is less than 3% of that obtained by solving Navier–Stokes equations. This observation indicates a very small effect of viscosity on the mass capture ratio. The maximum spillage of the mass appears to occur due to the phenomenon of side spillage.

Provision of fences or walls in the sides of a non-axisymmetric intake is suggested and used by many researchers[15,16] to reduce the amount of side spillage. In the present case also a side fence is provided stretching from the nose of the intake to the engine cowl lip. The schematic of the configuration is shown in Figure 6. Numerical simulations are carried out for

Table 3. Comparison of mass capture ratios from different simulations.

Case		Mass capture ratio (%)	Intake span (mm)	Flight Mach number	Flight altitude (km)
Krause and Ballmann[15]	Without side walls	55.56	76	8.0	30
	With side walls	79.22			
Nair et al.[14] (without side walls)	Case A (220 mm duct)	72.89	1600	6.5	35
	Case B (230 mm duct)	72.98			
	Case C (240 mm duct)	75.31			
Present Simulations	Without side walls	68.17	380	6.5	30
	With side walls	88.67			
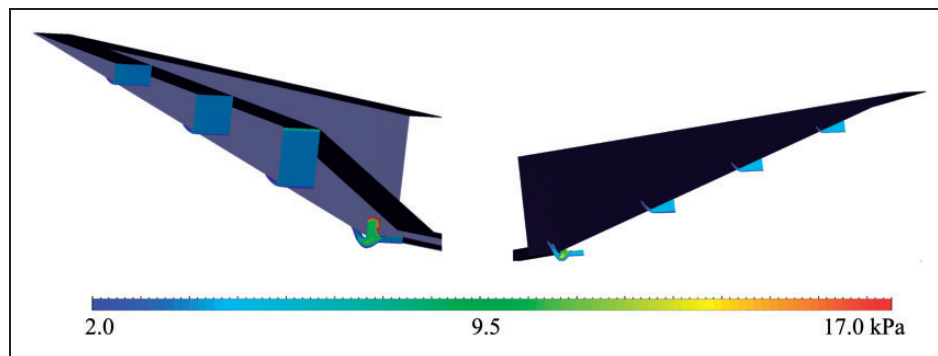
Figure 7. Static pressure distribution in span wise planes in presence of side wall.

the performance of the intake with side fences also. The evaluated mass capture ratio from the simulation results comes out to be around 88.67%. A comparison of mass capture ratio with geometric and flight conditions is shown in Table 3.

An examination of Table 3 in terms of mass capture ratios, with and without side wall, shows that there is a significant improvement in the mass capture ratio with introduction of side walls for both Krause and Ballmann[15] simulations as well for the present simulations. Presence of side wall physically stops the air flow from spilling to the sides. However, some amount of air does spill towards the sides in presence of side walls also. The static pressure distribution in span wise planes for the intake with side walls is shown in Figure 7. It can be noticed that the pressure distribution remains quite uniform as compared with the pressure distributions shown in Figure 5 for the intake geometry without side walls. Some amount of side flow does exist near the geometrical changes at the cowl and wall edges giving rise to corresponding higher mass capture ratio.

Considering the inlets without side walls, from the Table 3, it can be noticed that the mass capture ratio depends on the span of the inlet also. The inlet geometry considered by Nair et al.[14] has maximum span and shows maximum mass capture ratio without presence of side wall. The geometry considered in the present simulation without side walls shows lower mass capture ratio in comparison of Nair et al.[14] geometry.

The lowest mass capture ratio is observed in Krause and Ballmann[15] geometry which has lowest span also. From this data, it appears that the span of the intake is one of the important parameters for mass capture ratio value. The observation is also supported by the fact that theoretical mass capture ratio would be unity for an infinite span, as there would be no side spillage.

Finally, it is to be noticed that the mass capture ratios for all the cases shown in Table 3 are considerably less than 100%. However, the mass capture ratios from the stream thrust analysis are 100% at the design points. This significant decrease in actual mass capture ratio, due to side spillage, makes the use of the stream thrust analysis method to be flawed for even initial design and sizing purpose of a scramjet vehicle.

Apart from mass capture ratio, other flow parameters such as static and total pressures, static temperature, Mach number and velocity at the entry to supersonic combustion chamber are also of great concern. These flow parameters at some of the important planes are summarised in Table 4. The locations of the planes considered for the evaluation of the average values of these flow parameters are shown in Figure 1 on the schematic geometry of the scramjet engine. Plane 1 is located at the cowl of the engine after two oblique shocks from the nose and ramp turning. After the third shock and at the entrance of internal compression duct, plane 2 is located. The exit

Table 4. Flow parameters at different axial locations.

Parameter		Free stream	Plane 1 (after two shocks)	Plane 2 (after three shocks)	Plane 3 (after internal compression)	Plane 4 (after isolator)
Pressure (Pa)	One dimensional	1196	19041	85955	116385	116385
	Without side wall		12872	61199	93427	97240
	With side wall		19010	108796	159315	168724
Temperature (K)	One dimensional	227	580	943	1018	1018
	Without side wall		561	939	1092	1134
	With side wall		642	1201	1317	1344
Axial velocity (m/s)	One dimensional	1958	1685	1509	1420	1420
	Without side wall		1703	1461	1390	1361
	With side wall		1610	1262	1190	1166
Mach number	One dimensional	6.5	3.66	2.46	2.27	2.27
	Without side wall		4.06	2.47	2.10	2.03
	With side wall		3.50	1.95	1.70	1.65
Total pressure (bar)	One dimensional	31.03	18.18	13.90	13.89	13.89
	Without side wall		21.91	12.23	10.22	9.02
	With side wall		19.09	10.52	8.51	8.02
Axial location of the plane (m)			2.515	2.725	3.085	3.385

of internal compression is designated by plane 3. Plane 4 indicates end of isolator and entry to combustor. The axial locations from the nose tip of the vehicle are also shown in Table 4. The values of flow parameters computed by 1D method (stream thrust analysis), CFD methodology for without side wall geometry and with side wall geometry are shown together for comparison purpose in Table 4.

The values of static pressures at different locations are shown in Figure 8. It can be observed that the static pressures evaluated from 1D assumptions are always higher than that computed for without side wall configuration. These lower values of static pressures can be attributed to the 'leakage' through side spillage. When the side spillage is contained by the side walls, the pressures observed are higher than those calculated using 1D assumptions. The higher pressure occurs because of the additional deceleration of the flow due to presence of side wall. It can be clearly noticed that the intake geometry without side wall provides a lower static pressure at the combustor entry than evaluated through the 1D calculations while higher static pressure is observed for the geometry with side walls.

Static temperature values at different axial locations are graphically represented in Figure 9. The temperatures are highest for the geometry with side wall. The reason may be increased viscous effects due to presence of side wall. The higher temperature at the combustor entry may be a negative point for side wall geometries and needs to be analysed critically for design calculations.

Figure 10 shows the values of axial velocity at different axial locations. There are only small differences between ideal calculations and without side wall
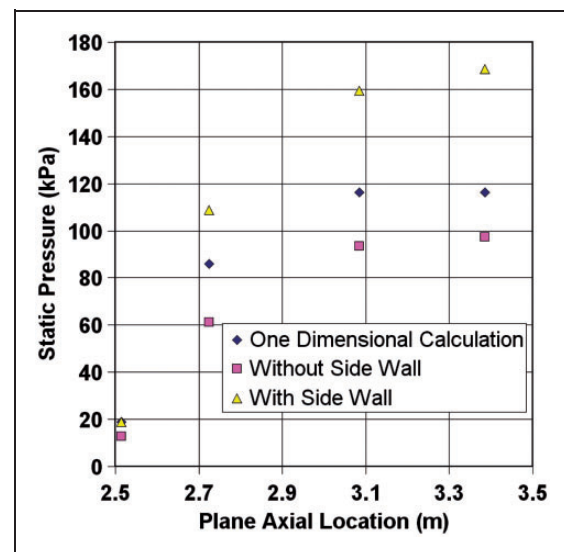
Figure 8. Average static pressures at different axial locations of the scramjet engine.

geometry arising mainly because of viscous effects. However, due to presence of side walls, these effects become more prominent and a larger decrease in the velocity is observed. This decrease in velocity is also manifested in the form of higher static pressures as shown in Figure 8.

Combustor entry Mach number is one of the most important parameters for a scramjet engine. The average values of flow Mach numbers are shown in Figure 11 at different axial locations. The value of average Mach number is lowest for the configuration with side walls, which could be a critical parameter for deciding in favor of a geometry.
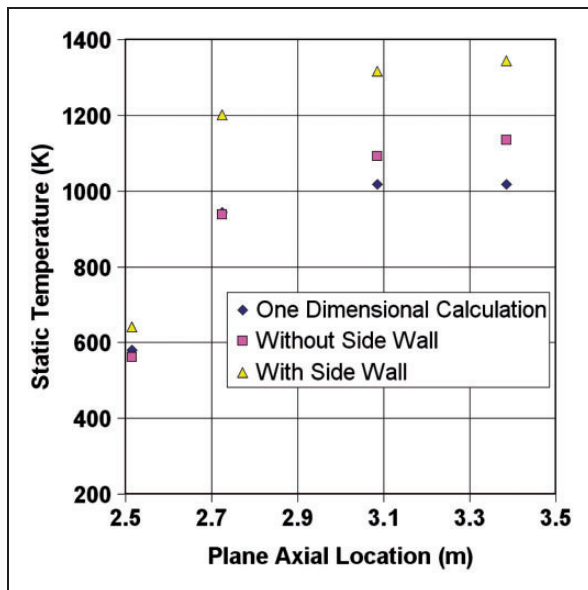
Figure 9. Average static temperatures at different axial locations of the scramjet engine.
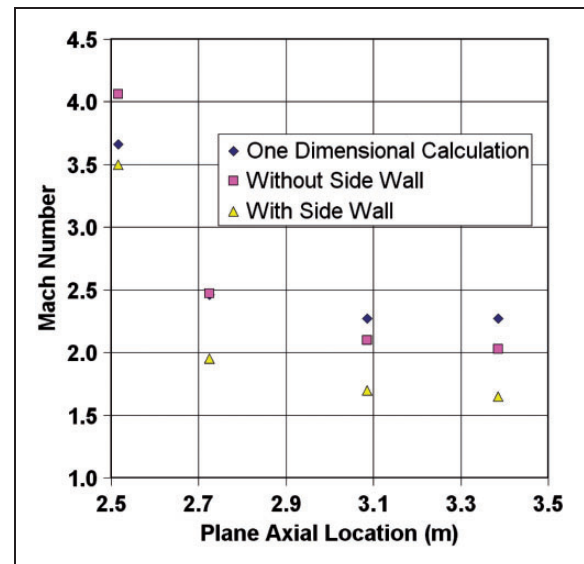
Figure 11. Average Mach numbers at different axial locations of the scramjet engine.
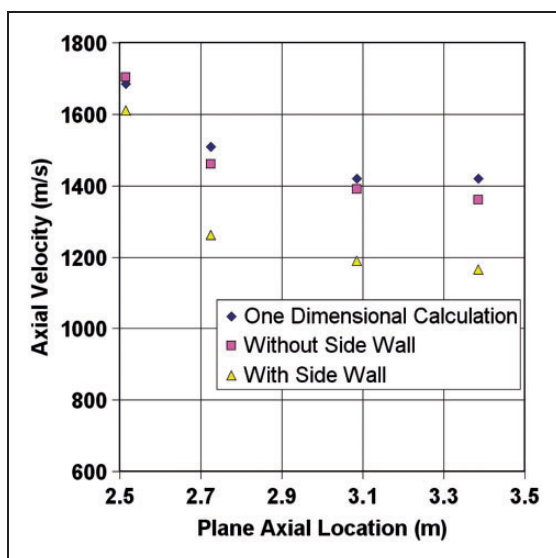
Figure 10. Average axial velocities at different axial locations of the scramjet engine.
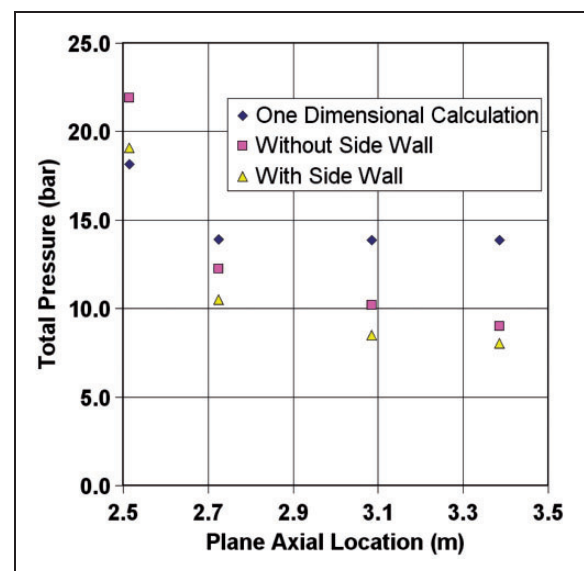
Figure 12. Average total pressures at different axial locations of the scramjet engine.

The total pressure represents the energy content of the flow and is shown at different axial locations in Figure 12. The examination of Figure 12 shows that the total pressure is lower than ideal calculations for both the computational geometries at all the locations except at plane 1. This can be explained in the view of occurrence of weaker oblique shocks due to viscous effects resulting in lesser losses due to shocks. At the combustor entry, around 11% lower total pressure is observed for the geometry with side walls.

It is seen from the Table 3, that the mass flow ratios are significantly lower for an actual non-axisymmetric intake due to presence of side spillage. The values of other important flow parameters viz. static and total

pressures, static temperature, Mach number and velocity at the entry to supersonic combustion chamber, also show considerable variation between those evaluated though the stream thrust analysis method and CFD computations, as observed from Table 4 and Figures 8 to 12. These observations indicate that a 3D CFD analysis is necessary even in the initial design and sizing phase of a scramjet vehicle with non-axisymmetric intake.

Conclusions

Numerical simulations are performed for a scramjet engine with airflow to compare the intake performance

with that evaluated using the stream thrust method. A severe loss in mass capture ratio without side walls is observed with a value of 68.17% due to side spillage only. A side wall is provided to contain the spillage and an improved mass capture ratio of 88.67% is calculated. The drastic fall in the mass capture ratio shows a drawback in the use of the stream thrust method for a non-axisymmetric geometry scramjet vehicle, due to omission of side spillage losses. Since, the stream thrust analysis and 2D CFD calculations do not account for the side spillage, their use even in preliminary design analysis is inadequate and complete 3D CFD studies are required for a non-axisymmetric scramjet engine.

Use of side wall or fences in the intake increases mass capture ratio and combustor entry static pressure and temperature, while decreasing Mach number, total pressure and velocity. These effects are to be considered while deciding for a particular geometry of the intake. Another important observation is reduction in side spillage with the increase in span of the intake. During the design optimisation, intakes with lower height and larger span may be designed for a higher mass capture ratio.

Declaration of Conflicting Interests

Funding

References

1. Curran ET and Craig RR. *The use of stream thrust concepts for the approximate evaluation of hypersonic ramjet engine performance*. AFAPL-TR-73-78, Aero Propulsion Laboratory, Wright-Patterson AFB, Dayton, OH, 1973.
2. Heiser WH and Pratt DT. *Hypersonic airbreathing propulsion*. Washington, DC: AIAA Inc, 1994, pp.173–192.
3. Akpolat MT, Toker KA and Genç MS. Design and optimization of a notional scramjet by means of stream thrust analysis and design of experiments. In: *19th AIAA international space planes and hypersonic systems and technologies conference*, AIAA 2014-2788, Atlanta, GA.
4. Rolim TC and Lu FK. Design and stream thrust analysis of a scramjet engine for acceleration mission from 2 to 3 km/s. In: *51st AIAA aerospace sciences meeting including the new horizons forum and aerospace exposition*, AIAA 2013-0120, Dallas, TX.
5. Roberts KN and Wilson DR. Analysis and design of a hypersonic scramjet engine with a transition mach number of 4.00. In: *47th AIAA aerospace sciences meeting including the new horizons forum and aerospace exposition*, AIAA 2009-1255, Orlando, FL.
6. Jain MK and Mittal S. Euler flow in a supersonic mixed-compression inlet. *Int J Numer Method Fluid* 2006; 50: 1405–1423.
7. Om Prakash Raj N and Venkatasubbaiah K. A new approach for the design of hypersonic scramjet inlets. *Phys Fluids* 2012; 24: 086103.
8. Blaize M, Knight D and Rasheed K. Automated optimal design of two-dimensional supersonic missile inlets. *J Propul Power* 1998; 14: 890–898.
9. Zha G-C, Smith D, Schwabacher M, et al. High-performance supersonic missile inlet design using automated optimization. *J Aircr* 1997; 34: 697–705.
10. Kim JW and Kwon OJ. Numerical simulation of supersonic inlet flow with movable cowl. *J Propul Power* 2015; 31: 1470–1472.
11. Ran H and Mavris D. Preliminary design of a 2D supersonic inlet to maximize total pressure recovery. In: *AIAA 5th ATIO and 16th lighter-than-air sys tech. and balloon systems conferences, aviation technology, integration, and operations (ATIO) conferences*, AIAA 2005-7357, Arlington, VA.
12. Hellman BM and Hartong AR. Conceptual level off-design scramjet performance modeling. In: *43rd AIAA/ASME/SAE/ASEE joint propulsion conference & exhibit*, AIAA Paper No. 2007-5031, Cincinnati, OH.
13. Nguyen T, Behr M, Reinartz B, et al. Effects of sidewall compression and relaminarization in a scramjet inlet. *J Propul Power* 2013; 29: 628–638.
14. Nair MT, Kumar N and Saxena SK. Computational analysis of inlet aerodynamics for a hypersonic research vehicle. *J Propul Power* 2005; 21: 286–291.
15. Krause M and Ballmann J. Numerical simulations and design of a scramjet intake using two different RANS solvers. In: *43rd AIAA/ASME/SAE/ASEE joint propulsion conference & exhibit*, AIAA 2007–5423, Cincinnati, OH.
16. Tani K, Kanda T, Kudo K, et al. Effect of sides-spillage from airframe on scramjet engine performance. *J Propul Power* 2001; 17: 139–145.
17. ICEM CFD-11. *Installation and overview*. Canonsburg, PA: ANSYS, 2007.
18. *ANSYS CFX 11.0, Ver. 11.0*. Canonsburg, PA: ANSYS, 2007.
19. Launder BE and Spalding DB. The numerical computation of turbulent flows. *Comp Meth Appl Mech Eng* 1974; 3: 269–289.
20. Manna P and Chakraborty D. Numerical investigation of transverse sonic injection in a nonreacting supersonic combustor. *Proc IMechE, Part G: J. Aerospace Engineering* 2005; 219: 205–215.
21. Manna P and Chakraborty D. Numerical investigation of confinement effect on supersonic turbulent flow past backward facing step with and without transverse injection. *J Aerospace Sci Techno* 2009; 61: 283–294.
22. Dharavath M, Sinha PK and Chakraborty D. Simulation of supersonic base flow – effect of computational grid and turbulence model. *ASME J Aerospace Eng* 2010; 224: 311–319.
23. Dharavath M and Chakraborty D. Numerical simulation of underexpanded sonic jet. *J Aerospace Sci Techno* 2012; 14: 259–267.
24. Aswin G and Chakraborty D. Numerical simulation of transverse side jet interaction with supersonic free stream. *J Aerospace Sci Techno* 2010; 14: 295–301.
25. Saha S, Rathod S, Chandra Murty MSR, et al. Numerical simulation of base flow of a long range flight vehicle. *Acta Astronaut* 2012; 74: 112–119.

26. Javed A, Manna P and Chakraborty D. Numerical simulation of dual pulse rocket motor flow field. *Defence Sci J* 2012; 62: 369–374.

27. Saha S, Sinha PK and Chakraborty D. CFD prediction of ramjet intake characteristics at angle of attack. In: *Proceedings of 8th national conference on air breathing engines and aerospace propulsion*, 12–14 December 2006. Pune, India: DIAT, pp.97–107.

28. Dharavath M, Manna P and Chakraborty D. Tip to tail simulation of a hypersonic airbreathing cruise vehicle. *J Propul Power* 2015; 31: 1370–1379.

29. Dharavath M, Manna P and Chakraborty D. Effect of turbulence models and spray parameters on kerosene fuelled scramjet combustor. *J Aerosp Sci Technol* 2015; 67: 369–383.